Aerospace Science and Technology 128 (2022) 107779

Contents lists available at ScienceDirect

Aerospace Science and Technology

www.elsevier.com/locate/aescte

Band-pass filtering analysis on low-frequency tonal noise generated from a Krueger storage cavity

Weishuang Lu [a,b,c,d], Peiqing Liu [a,b,c], Hao Guo [a,b,c,*]

[a] Key Laboratory of Aero-Acoustics (Beihang University), Ministry of Industry and Information Technology, Beijing, 100191, China
[b] Key Laboratory of Fluid Mechanics (Beihang University), Ministry of Education, Beijing, 100191, China
[c] School of Aeronautic Science and Engineering, Beihang University, Beijing, 100191, China
[d] Institute of Mechanics, Chinese Academy of Sciences, Beijing, 100190, China

ARTICLE INFO

Article history:
Received 14 April 2022
Received in revised form 23 June 2022
Accepted 18 July 2022
Available online 27 July 2022
Communicated by Yongle Du

Keywords:
Krueger flap
Storage cavity
Aero-acoustic
Noise characteristics
Band-pass filtering

ABSTRACT

With the aim of investigating noise characteristics of tonal noise generated from a Krueger storage cavity, aero-acoustic experiments on a two-dimensional, Krueger flap configuration with an open or closed gap were conducted in the D5 aero-acoustic wind tunnel at Beihang University. The angles of attack are from 4° to 8°, and the free-stream velocities are from 45 m/s to 60 m/s. To study further the noise temporal characteristics and generation mechanism, experimental results were analyzed using a band-pass filtering method. The results show that low-frequency noise generated by the Krueger storage flow is dominant when the Krueger flap is deployed without a gap. For the Krueger configuration with a closed gap, low-frequency multiple tones observed at a free-stream velocity above 45 m/s are generated by self-excited oscillation within the storage cavity. The frequencies corresponding to these tonal noises have an octave relationship and satisfy the Strouhal number related scaling law. Filtering results reveal further that these low-frequency tones are intermittently and alternately excited in time and satisfy the oscillation mode switching mechanism.

1. Introduction

The high-lift devices, as essential components for ensuring safety in the processes of take-off and landing, are significant contributors to the airframe noise [1–4], especially the leading-edge high-lift devices [5,6]. Currently, the comparatively common leading-edge high-lift devices include leading-edge slats, leading-edge droop noses (in service on Airbus A350, A380, etc. [7]), and leading-edge Krueger flaps (in service on Boeing B747, etc. [8]).

As one of the common high-lift devices, Krueger flaps are also considered necessary parts of high-lift system design for future aircraft [9]. With a potential increase in Krueger devices being used, the noise characteristics of the Krueger flaps have been studied in recent years [10,11]. Guo et al. [12] analyzed the noise characteristics to present a noise model, and mentioned that the noise components for Krueger flaps have similarities to slats.

Among them, low to mid frequency noise component is mainly generated by unstable flow in a cove of the leading-edge high-lift device, and amplified by fluid-acoustic feedback mechanism [13]. The aerodynamic and acoustic study [11] revealed that the noise generation mechanism of the slotted Krueger configuration is quite similar to that of a deployed slat due to their similar shapes. Krueger noise well matches slat noise in terms of maximum noise levels and spectral shape. Bahr et al. [14] conducted an aero-acoustic test of two types of leading-edge high-lift devices at multiple Mach numbers (Ma) and directivity angles to compare a conventional slat with a notional equivalent-mission Krueger flap. The results indicated that common behavior is observed between the conventional slat and the Krueger for both the low frequency tones and the broadband spectral components. Overall spectral scaling follows a $Ma^{4.5}$ power law when evaluated as a function of Strouhal number (St) for both devices [14]. Nevertheless, the noise generation mechanism for the Krueger flaps also has unique features [12]. Compared with a conventional slat configuration, there is a Krueger storage cavity on the lower side of the main wing, which opens when the Krueger flap is deployed. The noise generated by the unsteady flow in this cavity is also one of most significant noise component [12], apart from the noise due to gap flow [15], cove flow [16], and flow near brackets supporting the Krueger devices. Therefore, these four noise sources have been discussed and modeled by Guo et al. [12] to present a Krueger noise model. The results show that the gap and bracket noise are the strongest in the high frequency band, while the cav-

* Corresponding author at: School of Aeronautic Science and Engineering, Beihang University, Beijing, 100191, China.
E-mail address: guohao@buaa.edu.cn (H. Guo).

https://doi.org/10.1016/j.ast.2022.107779
1270-9638/

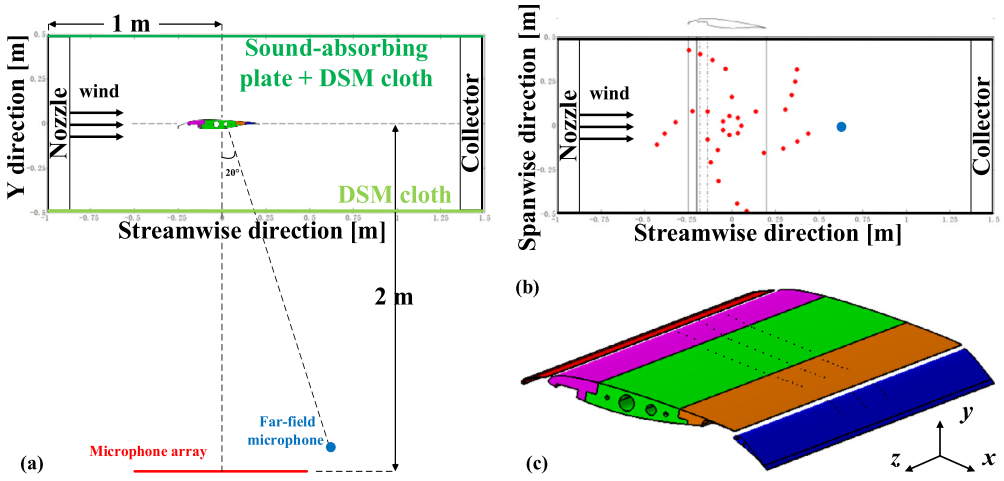

Fig. 1. Wind tunnel closed test section and model: (a) Top view of closed test section; (b) Side view of closed test section; (c) Schematic of experimental model. (For interpretation of the colors in the figure(s), the reader is referred to the web version of this article.)

ity and cove noise are the strongest in the low frequency or low to mid frequency band. Among them, the amplitude of the noise due to the cove flow is higher than that generated from the storage cavity flow. The Krueger storage cavity has a small influence on the model noise [14]. However, the Krueger flap can be deployed with or without gap [12], similar to the conventional slats. For a high-lift configuration model, completely sealing the gap leads to a dramatic reduction in acoustic levels of low to mid frequency noise due to the decrease of cove flow noise [14,17]. The cavity flow noise cannot be neglected when the gap is completely closed. Kreitzman et al. [18] simulated the sound field and flow field of a Krueger configuration with a closed gap, and found that sealing the gap between the leading-edge Krueger flap and the main wing tends to increase the importance of the cavity noise by increasing the unsteadiness near the storage cavity.

In addition, research results on cavity noise demonstrated that the appearance of multiple tones due to acoustic resonance [19,20] and self-excited oscillation phenomena (also known as fluid-acoustic feedback [21]) is one of significant acoustic phenomenon for the conventional cavities. For a cavity with a ratio of length over depth greater than 1, these tones are mainly generated from the fluid-acoustic feedback between unsteady flow in shear layer and acoustic waves [22,23]. Due to intermittency of the shear layer, multiple self-excited oscillation modes apparently coexist [24], and multiple tones simultaneously appear. Though there have been a number of studies focusing on the cavity noise, especially its tonal component [25,26], the Krueger storage cavity noise has not been extensively studied. In contrast to the conventional shallow cavities, the Krueger storage cavity commonly has an irregular geometric feature, which may define its noise characteristics. Secondly, the incoming condition of the storage cavity is not free-stream due to the existence of leading-edge high-lift devices. Hence, the acoustic phenomenon within the Krueger storage cavity may have its own unique characteristics.

Accordingly, the aim of this paper is to investigate noise characteristics of tonal noise generated from a Krueger storage cavity. The experiments were conducted in the D5 aero-acoustic wind tunnel at Beihang University. A high-lift configuration with a Krueger flap was used as experimental model. Corresponding experimental data were analyzed with a band-pass filtering method to analyze further the time-frequency characteristics of the narrowband noise generated from the Krueger storage cavity. The paper is organized as follows. Section 2 describes the methodology, including the experimental setup and the data analysis method. Section 3 presents and discusses the experimental results and the filtering analysis results. The conclusions are summarized in Section 4.

2. Methodology

2.1. Experimental facilities and test cases

Aero-acoustic measurements were conducted in the D5 aero-acoustic wind tunnel at Beihang University. The test section is 2.5 m in length with a square cross section of 1.0 m by 1.0 m. It is surrounded by an anechoic chamber to provide the non-reflecting condition. The anechoic chamber is 7 m (L) × 6 m (W) × 6 m (H), with a low cut-off frequency of $f = 200$ Hz [27]. The closed test section with semi-anechoic sidewalls was used in this paper, as shown in Fig. 1 (a), top view of the closed test section. The sidewall on the suction side consists of DSM Dyneema fiber (DSM) cloth tensioned with a sound-absorbing plate, while the sidewall on the pressure side is only a layer of DSM cloth [28]. When sound waves pass through the DSM cloth and the jet boundary layer, acoustic loss happens. The losses have been measured to correct the measured far-field sound pressure signals. The following results of the SPL have been corrected with DSM cloth and boundary layer losses.

As shown in Fig. 1, a free-field microphone and a microphone array were used as sound field measuring equipment. Far-field noise is measured using the Brüel & Kjær 12-channel acoustic vibration analysis system, which includes a 12-channel compact LAN-XI module and 1/2-inch free-field microphones (type 4189). The free-field microphone sensitivity is 50 mV/Pa, and dynamic range is 14.6 dB ∼ 146 dB. The acoustic signal is recorded over a time interval of 41.75 s at a sampling frequency of 65536 Hz. The microphone array is the KeyGo Tech multi-channel sound source localization system, which consists of 32 1/4-inch free-field microphones distributed spirally within a circle of 1 m in diameter. The microphones have a wide frequency range of 20 kHz and the dynamic range extends from 32 dB (A) to 135 dB. Acoustic data are processed at a particular frequency by the conventional beamforming algorithm.

The free-field microphone and the microphone array are placed at 2 meters away from the geometric center of the experimental model with direction angles of 290° and 270°, respectively. All the acoustic experimental instruments are located at the pressure side of model as in a flyover configuration, and its relative positions are shown in Fig. 1 (b). The red dots represent the relative position of the 32 microphones of the array, whilst the blue point depict the relative position of the free-field microphone.

Table 1
Geometrical settings of high-lift devices.

Configuration	Overlap [%C]	Gap [%C]	Rotation angle [°]	Chord length [%C]
Krueger flap	−0.77	1.01	148°	13.5
Closed-gap Krueger flap	0.48	0	148°	13.5
Trailing-edge flap	–	–	0°	18.0

Table 2
Geometrical settings of a Krueger storage cavity.

Parameters	Length [mm]
Cavity length, L	44.66
Leading edge depth, H_1	7.46
Trailing edge depth, H_2	15.93

Measurements of the mean surface pressure distribution on the high-lift configuration model are carried out by three electronic pressure scanners (Type PSI9816) with 0.05% in precision and every scanner can measure 128 pressure taps. 297 static pressure taps in total populate the airfoil surface, including all three cross sections along the spanwise direction, as shown in Fig. 1 (c), where there are 99 pressure taps in each cross section. Here, x is along the streamwise direction, y is along the vertical direction and z is along the spanwise direction. These taps are located along the mid-span cross section and other two cross sections, namely at z = 0 and 10% of the airfoil span length (b), respectively. The numbers of pressure tap on the main wing and flap surface in each cross section are 75 and 24, respectively. The leading-edge Krueger flap is too thin to set pressure taps. The reference pressure of the scanners is static free-stream pressure measured by a Pitot-static probe upstream.

Measurements are conducted at free-stream velocities (U_∞) from 45 m/s to 60 m/s corresponding to Reynolds numbers based on airfoil stowed chord (Re_c) from 1.22×10^6 to 1.62×10^6. The main wing angles of attack (AoAs) are from 4° to 8° with an interval of 1°.

2.2. Experimental model and its geometrical settings

As shown in Fig. 1 (c), a two-dimensional, three-element, high-lift configuration model was used as the experimental model in this paper, which is manufactured in aluminum alloy with 0.4 m stowed chord length and 1 m span length. The leading-edge Krueger flap and the trailing-edge flap chord lengths are, respectively, 13.5% and 18% of the airfoil stowed chord denoted as C. The rotation angle of the leading-edge Krueger flap is 148°. In order to avoid the influence of other noise sources, such as the trailing-edge flap, the flap is in a stowed situation. That is, the flap deflection angle is 0°. The geometrical settings of high-lift devices and a Krueger storage cavity are described in Table 1 and Table 2, respectively. The definitions of the geometrical settings are shown in Fig. 2.

The geometric center of the experimental model is 1 m from the nozzle, as shown in Fig. 1, and the experimental model is mounted vertically between two end-plates to ensure that the flow around the airfoil is two-dimensional.

2.3. Band-pass filtering method

A band-pass filter is a filter that passes frequency components in a certain frequency range, but attenuates frequency components in other ranges to a very low level. For an ideal band-pass filter, there should be a completely flat passband with no amplification or attenuation within, and all frequencies outside the passband are completely attenuated.

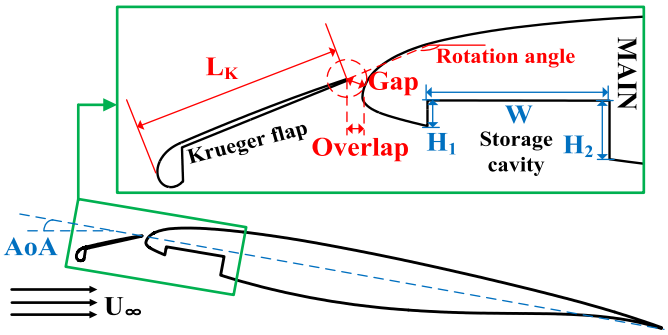

Fig. 2. The geometrical profiles of the tested high-lift configuration.

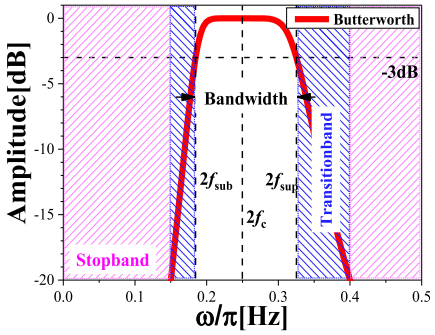

Fig. 3. Schematic of amplitude attenuation of a frequency response curve.

Fig. 3 shows the schematic of amplitude attenuation of Butterworth band-pass filter used in this paper. The center frequency f_c is 0.125 Hz and the passband width, difference between upper passband boundary (f_{sup}) and lower passband boundary (f_{sub}), is 0.12 Hz. Butterworth filters are known as maximum flat filters. The characteristic of an ideal Butterworth filter is that the frequency response curve plateaus maximally without ripples in the passband, gradually decreases to zero in the transition band (blue zone), and vanishes in the stopband (pink zone). In specific, bandwidth refers to the width of the frequency response curve when the amplitude is reduced by 3 dB, within which the passband lies. When the amplitude is reduced by more than 20 dB, the width is called the stopband (pink zone). The width of the frequency response curve with an amplitude reduction between 3 and 20 dB is called the transition band (blue zone).

2.4. 2D feature verification

Fig. 4 shows the experimental results of the surface pressure coefficient distribution of the model used in this paper at angles of attack of 4°, and 8°, respectively. The pressure distributions of the three spanwise cross sections have basically provided consistent results. This shows that the model generates 2D flows.

3. Results and discussion

3.1. Far-field noise characteristics of the Krueger high-lift configuration

Similar to a conventional slat, the Krueger flap can be deployed with or without gap [12]. Hence, the far-field noise characteris-

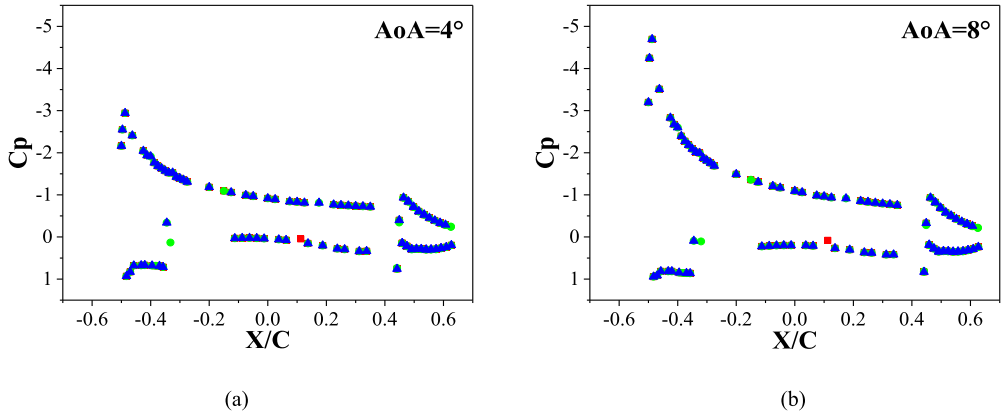

Fig. 4. Results of mean surface pressure distribution at freestream velocity of 50 m/s (Red square: experimental results at z/b = −0.1; Green circle: experimental results at z/b = 0; Blue triangle: experimental results at z/b = 0.1).

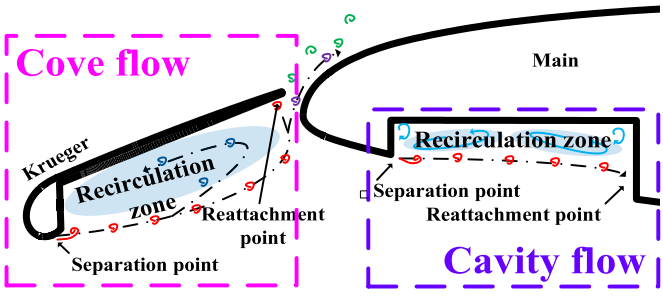

Fig. 5. Schematics of cove flow and cavity flow of the Krueger configuration with an open gap.

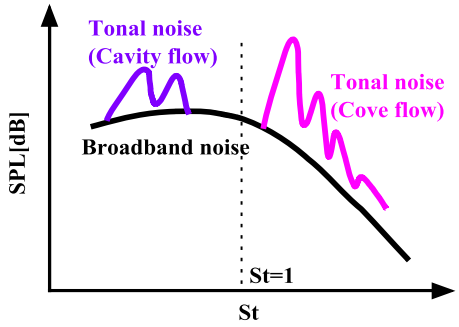

Fig. 6. Schematic diagram of frequency ranges of tonal noise predicted by the formula proposed by J. Rossiter [23] (St is Strouhal number for short).

tics of the Krueger configuration with and without gap are discussed first in this subsection. For the leading-edge Krueger configuration with a gap, a cove is formed between the leading-edge Krueger flap and the main wing. There are multiple tones superimposed on the low to mid frequency broadband noise due to the fluid-acoustic feedback within the cove. This noise generation mechanism has been fully discussed by analyzing the noise characteristics of the leading-edge slat configurations [29,30]. In addition, there is a Krueger storage cavity on the lower side of the main wing. According to its geometrical settings mentioned above, this cavity can be regarded as a square shallow cavity, and fluid-acoustic feedback phenomenon may also occur in this cavity [23]. As shown in Fig. 5, red lines represent the vortices in shear layers, blue lines represent the vortices in recirculation zones and black dashed lines represent mean streamlines. Fig. 6 shows the frequency ranges of tonal noise generated by the cove flow and cavity flow, which are predicted by the formula proposed by J. Rossiter [23], as shown in Eq. (1).

$$St = \frac{fL}{U_\infty} = \frac{n-\alpha}{U_\infty/U_c - Ma} \tag{1}$$

where, n is an integer used to represent the number of vortices in the shear layer. α is the phase delay coefficient that is related to the time delay between the vortex reaching the impact corner and the sound pulse radiating out. L is the characteristic length of the cove or the storage cavity. U_c is the convection velocity in the shear layer. Ma is the ratio of the free-stream velocity (U_∞) to the speed of sound.

The gap flow increases the convection velocity in the shear layer between the main wing and the Krueger flap, which is much higher than the convection velocity in the storage cavity. Hence, the frequency range of tonal noise generated by the cove flow is higher than that by the cavity flow.

Fig. 7 shows the far-field noise spectra of the Kruger configuration at different angles of attack when the free-stream velocity is 50 m/s. It can be seen that, for the Krueger configuration with a gap, obvious multiple tones appear in both the low and the low to mid frequency bands. According to the mentioned above, the generation mechanism of the low to mid frequency tonal noise generated from the slotted Krueger configuration is due to the self-excited oscillation within the cove [11]. The frequency range corresponding to the tonal noise can be better predicted by the formula proposed by M. Terracol [29], and its amplitude is related to the self-excited oscillation mode selection [31]. When the gap between the Krueger flap and the main wing is closed, the acoustic levels of both tonal noise and broadband noise in the low to mid frequency decrease significantly, and the amplitude of the low-frequency narrowband noise increases slightly. This is consistent with previous research results [18]. It should be noted that narrowband noise occurs at low frequencies, regardless of whether the Krueger flap is deployed with or without a gap, and the corresponding frequencies to these narrowband noises are in the same frequency bands. This shows that, for the Krueger high-lift configuration studied in this paper, there exists the same noise generation mechanism no matter whether the gap is closed or not, and it produces obvious narrowband noise in the low frequency band. Moreover, due to the closure of the gap, the flow phenomenon in the Krueger cove has changed dramatically [14,17], so it can be assumed that the noise generation mechanism should be almost independent of the fluid-acoustic feedback phenomenon in the cove. To analyze further the noise source characteristic of the low-frequency narrowband noise, noise source localization analysis is performed at angles of attack of 4°, 6° and 8°, with the results being shown in Fig. 8 and Fig. 9.

As shown in Fig. 8, the noise source maps of the leading-edge Krueger flap configuration with a gap at frequencies of 1 kHz and 3 kHz, the sound sources are located near the leading-edge high-lift

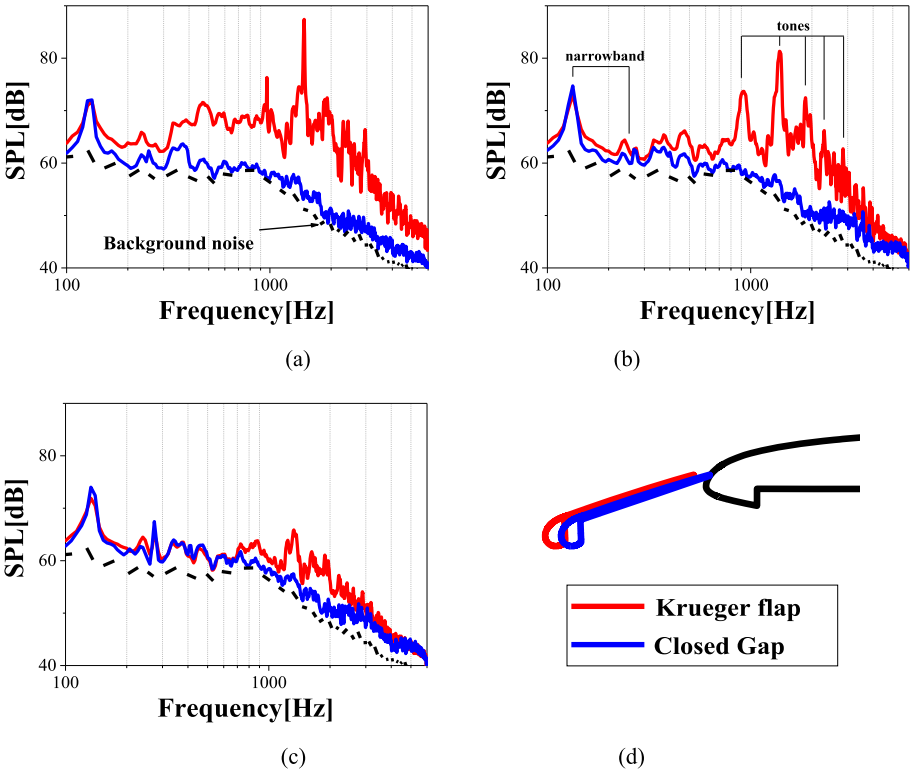

Fig. 7. Far-field noise spectra of high-lift configurations with Krueger flap at the incoming speed of 50 m/s((a): AoA = 4°, (b) AoA = 6°, (c) AoA = 8°, (d): Schematic diagram of geometric settings).

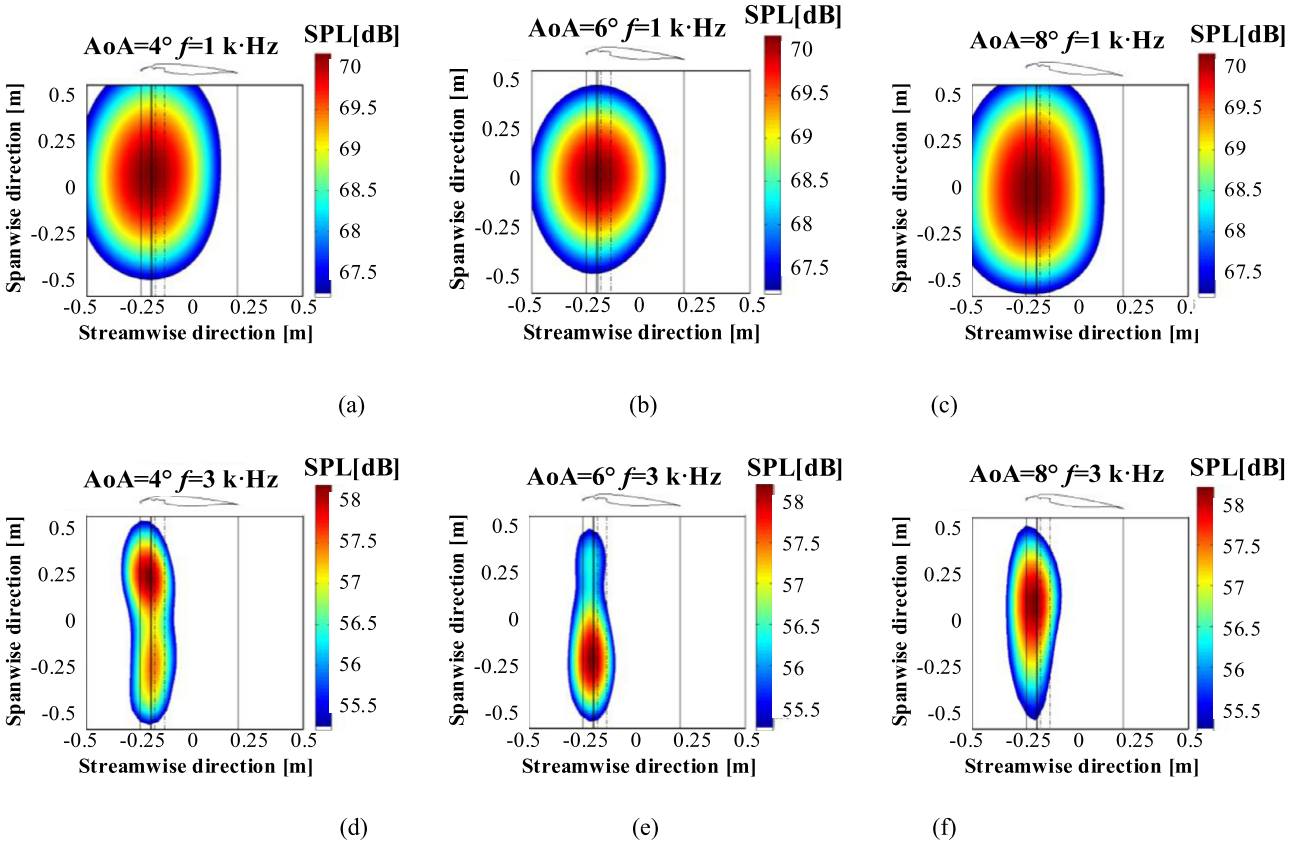

Fig. 8. Noise source maps of the high-lift configuration with a Krueger flap.

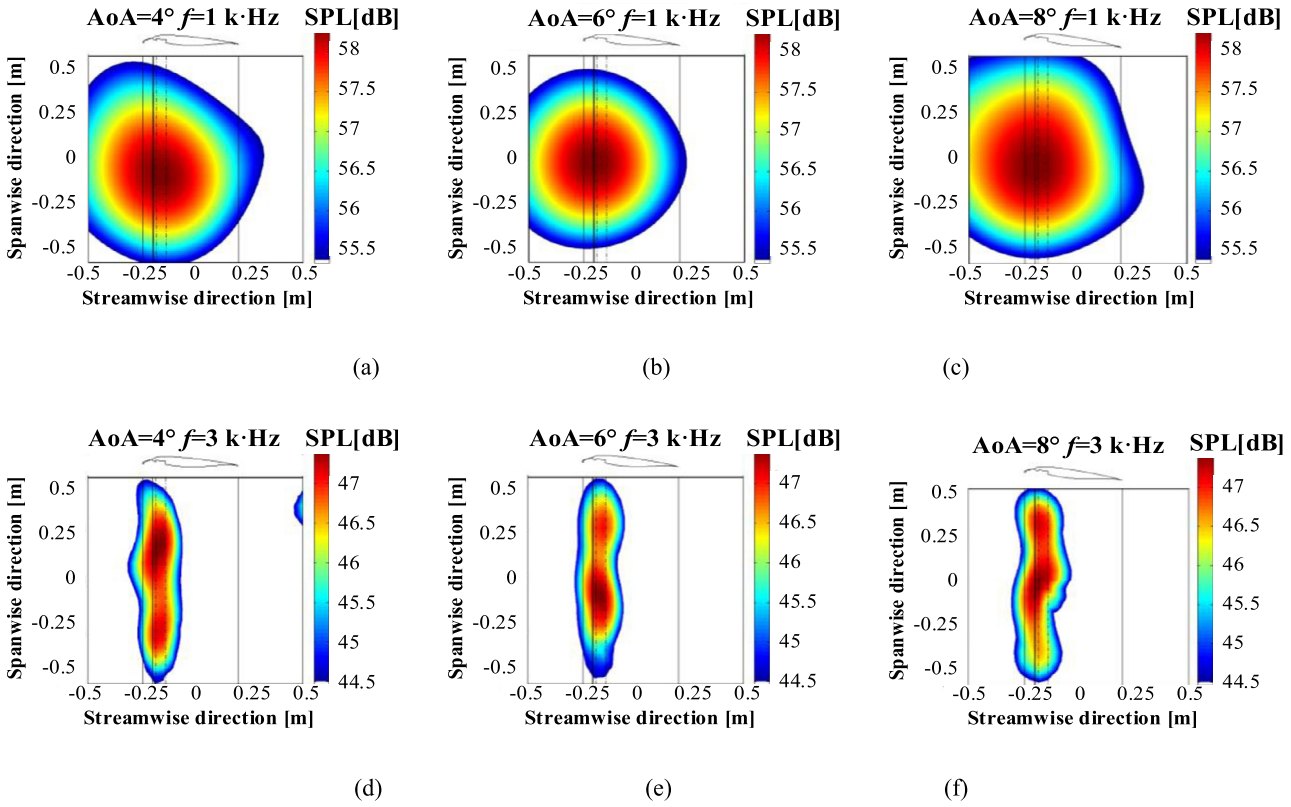

Fig. 9. Noise source maps of the high-lift configuration with a closed-gap Krueger flap.

device. When the analysis frequency is 1 kHz, because the conventional beamforming algorithm has a low spatial resolution at low frequencies, the sound source location is not clear. However, it can be seen that the sound source location is basically at the gap between the Krueger flap and the main wing. When the analysis frequency is 3 kHz, it can be seen that the sound source location is in the vicinity of the Krueger cove. This indicates that the noise generated by Krueger cove flow is the strongest for the Krueger flap configuration with a gap.

Fig. 9 shows the noise source localization analysis results of the Krueger flap configuration with a closed gap. It can be seen that the sound source location is still near the leading edge high-lift device. Compared with Fig. 8, the sound source location is closer to the Krueger storage cavity for the configuration with a closed gap. When the analysis frequency is 3 kHz, it can be seen that the sound source location is basically in the vicinity of the storage cavity. This shows that the noise generated by the cavity is stronger when the Krueger flap is deployed without a gap.

Based on the analysis of the far-field noise and noise source localization above, it can be seen that, after the gap is closed, the low to mid frequency noise generated by the Krueger cove flow greatly decreases, and the low-frequency narrowband noise generated by the storage cavity flow slightly increases. The low-frequency narrowband noise generation mechanism may be the self-excited oscillation within the Krueger storage cavity.

3.2. Low-frequency narrowband noise generated from the Krueger storage cavity

The analysis results in the previous subsection show that the noise is mainly generated from the Krueger storage cavity, when the gap between the Krueger flap and the main wing is closed. Hence, low-frequency noise characteristics of the Krueger configuration with a closed gap are analyzed in this subsection to verify

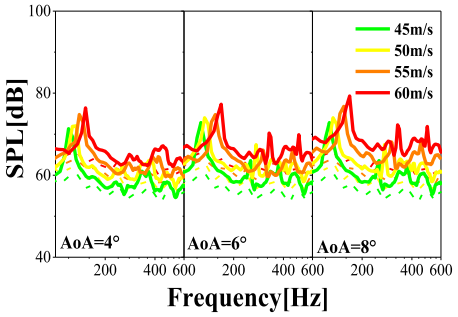

Fig. 10. Far-field noise results at different AoAs and free-stream velocities.

further the noise generation mechanism of the low-frequency narrowband noise generated from the storage cavity.

Fig. 10 shows the low-frequency noise spectrum of the Krueger high-lift configuration with a closed gap at different AoAs and free-stream velocities. The AoAs are 4°, 6° and 8°, and the free-stream velocities are from 45 m/s to 60 m/s, with an interval of 5 m/s. Solid lines represent the model noise spectrum curves, and dashed lines represent the background noise spectrum curves. As shown in Fig. 10, there is tonal noise superimposed on the low-frequency broadband noise. The amplitude of low-frequency broadband noise increases as the free-stream velocity increases from 45 m/s to 60 m/s.

As shown in Fig. 11, there is obvious tonal noise superimposed on the low-frequency broadband noise. The frequencies corresponding to these tones are hardly affected by the increase of the AoA. However, the amplitude of the low frequency broadband noise increases slightly as the AoA increases. Fig. 12 shows the far-field noise results at an AoA of 8° and high free-stream velocities. It can be seen in the left one of Fig. 12 that the frequencies corresponding to the tones move to high frequency bands as the

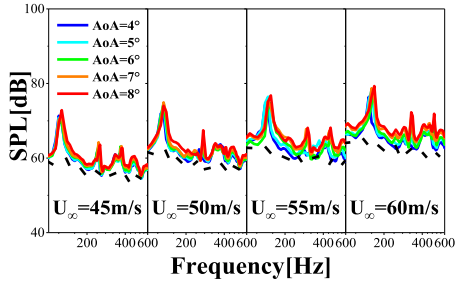

Fig. 11. Effect of the AoAs on model noise.

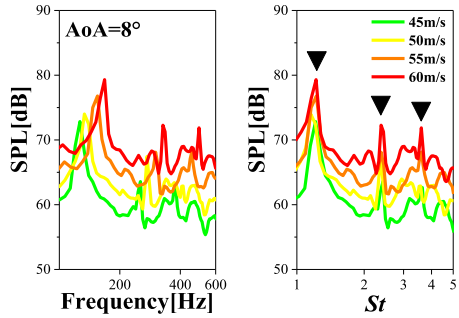

Fig. 12. Far-field noise results and its normalized analysis at an AoA of 8 °.

free-stream velocity increases, which is also observed from Fig. 10. In addition, normalized tonal frequency results are plotted in the right one of Fig. 12. The tonal frequencies are normalized using the Strouhal number (St), which is based on the cavity length L and the free-stream velocity U_∞ as $St = f \cdot L/U_\infty$. The normalized tonal frequencies are the same in all high free-stream velocity cases. This indicates that the tonal frequencies are proportional to the free-stream velocity, and these tones satisfy the St scaling law. The St scaling law also implies that the dominant tonal noise generation mechanism is the self-excited oscillation mechanism.

Based on the analysis above, there are obvious tones at low frequency band, and the frequencies corresponding to the tones are proportional to the free-stream velocity. Nevertheless, these tonal frequencies are hardly affected by the increase of the AoA. These features indicate that the low-frequency tonal noise is caused by the self-excited oscillation phenomenon within the Krueger storage cavity.

3.3. Filtering analysis results of low-frequency narrowband noise

To reveal further the noise generation mechanism, the temporal characteristics of low-frequency narrowband noise generated from the storage cavity at an AoA of 8° and free-stream velocities of 45 m/s, and 55 m/s are analyzed using a band-pass filtering method in this subsection. The frequencies corresponding to low-frequency narrowband noise (f_{ci}, where $i = 1, 2, 3$) as well as the frequency spacings (Δf_c) are summarized in Table 3. Limited by the cut-off frequency of the wind tunnel, the filtering analysis is performed only on the noise data corresponding to f_{c2} and f_{c3} at each free-stream velocity. It can be seen from Table 3 that the frequencies corresponding narrowband noise have an octave relationship when the free-stream velocity is 45 m/s or 55 m/s.

As shown in Fig. 13, the left side is the time-averaged noise spectrum, and the right side is the filtering results with the center frequencies of $f_{c2} = 256$ Hz and $f_{c3} = 382$ Hz, respectively, where the filtering bandwidth is 80 Hz and 60 Hz, respectively. The solid black line on the right side of Fig. 13 represents conditional statistics results of the sound pressure amplitude, Γ, which is defined as in Eq. (2)

Table 3
Frequencies corresponding to low-frequency narrowband noise.

i	U = 45 m/s		U = 55 m/s	
	f_{ci}	$\Delta f_c = f_{ci+1} - f_{ci}$	f_{ci}	$\Delta f_c = f_{ci+1} - f_{ci}$
1	126	130	154	152
2	256	126	306	156
3	382		462	

$$\Gamma(t) = \begin{cases} 1 & \text{if } |A| > 0.75 \cdot |A_{max}| \\ 0 & \text{if } |A| \le 0.75 \cdot |A_{max}| \end{cases} \quad (2)$$

where A is the sound pressure amplitude, $|A_{max}|$ is the absolute value of maximum sound pressure amplitude, and $\Gamma(t)$ is the conditional function. It is assumed that the narrowband noise occurs when Γ is equal to 1; when Γ is 0, the noise is considered as not be excited.

Fig. 13 shows that the two noises analyzed basically are excited intermittently. The appearance of f_{c2} generally corresponds to the absence of f_{c3} instead of being excited simultaneously, except for some small time intervals when both tones are absent or present. According to the principle of shallow cavity self-excited oscillation, self-excited oscillation noise is generated by the interaction between the vortex in the shear layer at the front edge and the solid wall at the rear edge of the cavity. A stable phase relationship occurs between the upstream and downstream solid surfaces, finally forming a mutual feedback between flow and sound [32]. The characteristic frequencies of the self-excited oscillation noise are related to a feedback loop involving the shedding of flow instabilities at front edge which are advected in the downstream direction, and upstream propagating acoustic waves generated by the interaction with the solid wall at the rear edge, which in turn excite new instabilities as they arrive at the upstream solid surface [33]. Due to the instabilities, there are multiple frequencies or modes of the self-excited oscillation noise. The dominant energy in the feedback loop switches from one mode to another, jumping between the different modes [24,34]. Hence, the tones at f_{c2} and f_{c3} are excited alternately.

Fig. 14 shows the results when the free-stream velocity is 55 m/s. Similar to the results of Fig. 13, the tonal noise at $f_{c2} = 306$ Hz and $f_{c3} = 462$ Hz are intermittently and alternately excited. This indicates that, at a free-stream velocity of 55 m/s, the low-frequency tonal noise of interest is also generated by the self-excited oscillation within the Krueger storage cavity.

From analysis results above, the frequencies corresponding the low-frequency tones have an octave relationship. The tones are intermittently and alternately excited, according to the principle of shallow cavity self-excited oscillation. These illustrate further that the low-frequency tones are generated by the self-excited oscillation within the Krueger storage cavity.

4. Conclusions

Time-averaged noise spectra and noise source localization location results show that characteristic frequencies of the tones generated due to the Krueger cove flow are at the low to mid frequencies, and characteristic frequencies of the tones generated by the storage cavity flow are usually at low frequencies. The low to mid frequency noise generated by the Krueger cove flow drops sharply, and the low-frequency noise generated from the Krueger storage cavity is dominant when the Krueger flap is deployed without a gap.

By analyzing further the low-frequency noise results at different angles of attack and free-stream velocities, it has been found that the angle of attack has little effect on the corresponding frequencies and amplitudes of the low-frequency tonal noise. Nevertheless, the free-stream velocity has a significant effect on noise

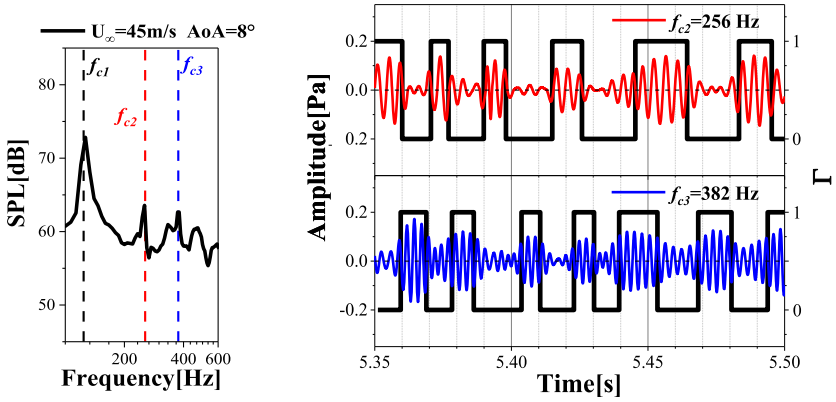

Fig. 13. Band-pass filtering analysis results at a free-stream velocity of 45 m/s.

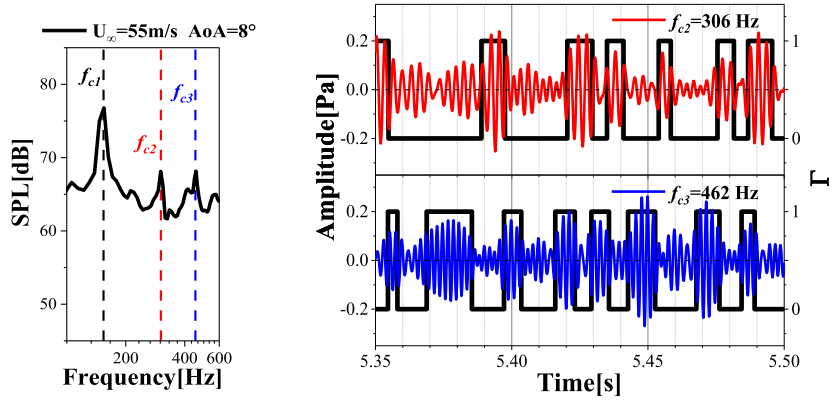

Fig. 14. Band-pass filtering analysis results at a free-stream velocity of 55 m/s.

characteristics. At free-stream velocities ranging from 45 m/s to 60 m/s, there are obvious tones at the low frequency band, and the frequencies corresponding to the tones are proportional to the free-stream velocity and satisfy the *St* scaling law. These features indicate that the low-frequency tonal noise is generated by the self-excited oscillation phenomenon within the Krueger storage cavity.

Band-pass filtering results reveal further the temporal characteristics and generation mechanism of the low-frequency tonal noise. The tones are intermittently and alternately excited and the dominant acoustic energy switches from one mode to another, jumping between the different modes. The low-frequency tonal noise is generated from the self-excited oscillation and satisfies the mode switching mechanism. Filtering analysis method demonstrates further that, at a free-stream velocity above 45 m/s, the dominant tonal noise generation mechanism is the self-excited oscillation mechanism.

Declaration of competing interest

The authors declare that they have no known competing financial interests or personal relationships that could have appeared to influence the work reported in this paper.

Data availability

Data will be made available on request.

Acknowledgements

This work was supported by the National Natural Science Foundation of China (Grant No. 12072016, 1217021666, 11772033 and 11721202).

References

[1] W. Dobrzynski, Almost 40 years of airframe noise research: what did we achieve?, J. Aircr. 47 (2) (2010) 353–367.
[2] M.Y. Zhang, A. Filippone, Optimum problems in environmental emissions of aircraft arrivals, Aerosp. Sci. Technol. 123 (2022) 107502.
[3] R. Merino-Martinez, J. Kennedy, G.J. Bennett, Experimental study of realistic low–noise technologies applied to a full–scale nose landing gear, Aerosp. Sci. Technol. 113 (2021) 106705.
[4] R. Merino-Martinez, E. Neri, M. Snellen, et al., Multi-approach study of nose landing gear noise, J. Aircr. 57 (3) (2020) 517–533.
[5] Y.P. Guo, M.C. Joshi, Noise characteristics of aircraft high lift systems, J. Aircr. 41 (7) (2003) 1247–1256.
[6] G.Y. Chen, X.L. Tang, X.Q. Yang, et al., Noise control for high-lift devices by slat wall treatment, Aerosp. Sci. Technol. 115 (2021) 106820.
[7] H.P. Monner, M. Kintscher, T. Lorkowski, et al., Design of a Smart Droop Nose as Leading Edge High Lift System for Transportation Aircraft, 50th AIAA/ASME/ASCE/AHS/ASC Structures, Structural Dynamics, and Materials Conference, Palm Springs, California, AIAA paper 2009-2128, Palm Springs, California, 2009.
[8] Michael Chun-Yung Niu, Mike Niu, Airframe Structural Design – Practical Design Information and Data on Aircraft Structures, Lockheed Aeronautical Systems Company CONMILIT PRESS Ltd., Burbank, California, ISBN 962-7128-04-X, 1988.
[9] J.T. Bonet, H.G. Schellenger, B.K. Rawdon, et al., Environmentally Responsible Aviation (ERA) Project – N+2 Advanced Vehicle Concepts Study and Conceptual Design of Subscale Test Vehicle (STV), NASA Contract Report, December 2011.
[10] R.H. Thomas, C.L. Burley, E.D. Olson, Hybrid wing body aircraft system noise assessment with propulsion airframe aeroacoustic experiments, Int. J. Aeroacoust. 11 (3+4) (2012) 369–410.
[11] M. Pott-Pollenske, D. Almoneit, J. Wild, On the Noise Generation of Krueger Leading Edge Devices, 21st AIAA/CEAS Aeroacoustics Conference, Dallas, TX, 22-26, AIAA Paper 2015-3142, June 2015.
[12] Y. Guo, C.L. Burley, R.H. Thomas, Modeling and Prediction of Krueger Device Noise, 22nd AIAA/CEAS Aeroacoustics Conference, Lyon, France, AIAA Paper 2016-2957 2016.
[13] W. Li, Y. Guo, W. Liu, On the mechanism of acoustic resonances from a leading-edge slat, Aerosp. Sci. Technol. 113 (2021) 106711.

[14] C.J. Bahr, F.V. Hutcheson, R.H. Thomas, et al., A Comparison of the Noise Characteristics of a Conventional Slat and Krueger Flap, 22nd AIAA/CEAS Aeroacoustics Conference, Lyon, France, AIAA paper 2016-2961, 2016.
[15] T. Imamura, S. Enomoto, Y. Yokokawa, et al., Three-dimensional unsteady flow computations around a conventional slat of high-lift devices, AIAA J. 46 (5) (2008) 1045–1053.
[16] C.C. Pagani, D.S. Souza, M.A.F. Medeiros, Experimental investigation on the effect of slat geometrical configurations on aerodynamic noise, J. Sound Vib. 394 (2017) 256–279.
[17] M. Herr, M. Pott-pollenske, R. Ewert, et al., Large-Scale Studies on Slat Noise Reduction, 21st AIAA/CEAS Aeroacoustics Conference, Dallas, TX, AIAA paper 2015-3140, 22–26 June 2015.
[18] J. Kreitzman, R. Cheng, N.J. Moffitt, et al., A Qualitative Acoustic Analysis of Krueger Device Noise Utilizing CFD/CAA Experiments, 23rd AIAA/CEAS Aeroacoustics Conference, Denver, Colorado, AIAA paper 2017-3365, 5-9 June 2017.
[19] M. Meissner, Experimental investigation of discrete sound production in deep cavity exposed to airflow, Arch. Acoust. 18 (1) (1993) 131–156.
[20] R. Merino-Martinez, M. Snellen, Implementation of tonal cavity noise estimations in landing gear noise prediction models, AIAA AVIATION 2020 FORUM, 15 - 19 June 2020, Online event.
[21] S.A. Elder, T.M. Farabee, F.C. DeMetz, Mechanisms of flow-excited cavity tones at low Mach number, J. Acoust. Soc. Am. 72 (2) (1982) 532–549.
[22] D. Rockwell, C. Knisely, The organized nature of flow impingement upon a corner, J. Fluid Mech. 93 (1979) 413–432.
[23] J.E. Rossiter, Wind-Tunnel Experiments on the Flow over Rectangular Cavities at Subsonic and Transonic Speeds, Aeronautical Research Council Reports and Memoranda, RAE Technical Report No. 64037, Ministry of Aviation; Royal Aircraft Establishment, RAE Farnborough, 1964.
[24] D. Rockwell, Oscillations of impinging shear layers, AIAA J. 21 (5) (1983) 645–664.
[25] V. Sarohia, Experimental investigation of oscillations in flows over shallow cavities, AIAA J. 15 (7) (1977) 984–991.
[26] S.A. Elder, Forced oscillations of a separated shear layer with application to cavity flow-tone effects, J. Acoust. Soc. Am. 67 (3) (1979) 774–781.
[27] P. Liu, Y. Xing, H. Guo, et al., Design and performance of a small-scale aeroacoustic wind tunnel, Appl. Acoust. 116 (2017) 65–69.
[28] W. Lu, P. Liu, H. Guo, et al., Investigation on tones due to self-excited oscillation within leading-edge slat cove at different angles of attack: frequency and intensity, Aerosp. Sci. Technol. 91 (2019) (2019) 59–69.
[29] M. Terracol, E. Manoha, B. Lemoine, Investigation of the unsteady flow and noise generation in a slat cove, AIAA J. 54 (2) (2017) 1–21.
[30] M. Terracol, E. Labourasse, E. Manoha, et al., Numerical simulation of the 3D unsteady flow in a slat cove for noise prediction, 9th AIAA/CEAS Aeroacoustics Conference and Exhibit, 12–14 May 2003, Hilton Head, South Carolina, AIAA Paper 2003-3110, 2003.
[31] W. Lu, P. Liu, H. Guo, et al., Investigation on tones due to self-excited oscillation within the leading-edge slat cove at different incoming flow speeds, Appl. Acoust. 155 (2019) (2019) 232–239.
[32] C.K.W. Tam, T.D. Norum, Impingement tones of large aspect ratio supersonic rectangular jets, AIAA J. 30 (2) (1992) 304–311.
[33] Y.P. Tang, D. Rockwell, Instantaneous pressure fields at a corner associated with vortex impingement, J. Fluid Mech. 126 (1983) 187–204.
[34] S. Ziada, D. Rockwell, Generation of higher harmonics in a self-oscillating mixing layer-wedge system, AIAA J. 20 (2) (1982) 196–202.